Journal of
Micro/Nanolithography,
MEMS, and MOEMS

SPIEDigitalLibrary.org/jm3

Propagation of surface topography of extreme ultraviolet blank substrate through multilayer and impact of phase defect structure on wafer image

Tsuyoshi Amano
Tsuneo Terasawa

SPIE

Propagation of surface topography of extreme ultraviolet blank substrate through multilayer and impact of phase defect structure on wafer image

Tsuyoshi Amano
Tsuneo Terasawa
EUVL Infrastructure Development Center, Inc.
16-1 Onogawa, Tsukuba-shi
Ibaraki-ken 305-8569, Japan
E-mail: tsuyoshi.amano@eidec.co.jp

Abstract. Our recent study reveals that the propagation of a phase defect (PD) from an extreme ultraviolet mask substrate surface through a multilayer does not always propagate in a vertical direction. To fully understand the propagation model of PDs, two types of defects on a quartz (Qz) substrate are prepared. One is space patterns fabricated by a mask patterning process followed by an etching giving a cross-sectional angle of 90 deg. The others are atomic force microscopy scratched space patterns with their cross-sectional angles as 30 deg and 60 deg. After coating a patterned Qz substrate with a multilayer, propagation of PDs through the multilayer was observed by a transmit electron microscope (TEM). As a result, the TEM images clearly exhibit a tendency that originates from the Qz substrate while the PDs propagate through the multilayer and their propagation path is inclined toward the center of the mask. The impacts of the inclination angles on the printed images on a wafer are calculated using a simulator. A PD with an inclination angle of 1 deg corresponds to a positional shift of 1 nm on a printed wafer image. © *The Authors. Published by SPIE under a Creative Commons Attribution 3.0 Unported License. Distribution or reproduction of this work in whole or in part requires full attribution of the original publication, including its DOI.* [DOI: 10.1117/1.JMM.12.3.033015]

Subject terms: extreme ultraviolet; phase defect; defect mitigation; compensation repair.

Paper 13033P received Mar. 21, 2013; revised manuscript received Jul. 16, 2013; accepted for publication Jul. 22, 2013; published online Aug. 30, 2013.

1 Introduction

The influence of phase defect (PD) embedded in extreme ultraviolet (EUV) mask blanks on wafer printing has always been an area of major interest among the device and mask makers.[1–6] There have been a number of techniques reported to minimize the printability of PDs. One proposed method is to cover the PDs beneath the absorber layer by shifting the location of the device pattern during mask patterning.[7–12] The other one is to eliminate the influence of the phase error by removing the absorber from the close proximity of the PDs after fabricating the device pattern.[13] Regarding these elimination methods, it is necessary to fully understand the effects of multilayer geometry of the PDs and size of PDs on wafer printing.[14,15]

As for the growth model of a PD resulting from some bumps or pits on a substrate, a number of transmit electron microscope (TEM) images of PDs have indicated that the growth of PD originating from the substrate surface does not always propagate in a vertical direction.[16–18] This means that the multilayer surface geometry measurement of PDs using atomic force microscopy (AFM) or nonactinic system may not identify a defect position correctly and thus may not be the right tools for defect mitigation strategy of covering or compensating for the PDs by absorber pattern. Therefore, to efficiently cover the PDs by an absorber layer, it is necessary to take into account the cross-sectional shape of the PDs and analyze their impacts using high resolution actinic imaging tool like an actinic blank inspection tool or an aerial image measurement system.[19]

In this article, to fully understand the defect propagation from the surface of a substrate through the multilayer, several types of defects were fabricated on the substrate. Some such defects were then observed by using TEM after coating the substrate with a multilayer. Using a lithography simulator, the impact of the PD structure on wafer images was also calculated.

2 Experimental Condition

2.1 *Preparation of the Qz Substrate with Various Shapes of Space Patterns*

The cross-sectional angles of the space patterns on the quartz (Qz) substrate were designed to be 90 deg, 60 deg, and 30 deg. The 90 deg space pattern was fabricated by applying a standard resist patterning on Qz, followed by a dry etching process. The space patterns with 60 deg and 30 deg angles were fabricated by applying scratch markers on the Qz substrate using an AFM tip with the tip angles of 60 deg and 30 deg as shown in Fig. 1(a). By pressing the tip against the Qz surface, five scratch lines were drawn as shown in Fig. 1(b). A cross-sectional profile of Fig. 1(b) along a line between two illustrated arrows is shown in Fig. 1(c).

Figure 2(a) shows the mask design. Space patterns with their etching angles of 90 deg were arrayed in a 7×7 matrix with a pitch of 22 mm on the Qz substrate. Each block has 150-nm-wide space patterns with their orientation angles of 0 deg, 45 deg, 90 deg, and 135 deg forming an asterisk symbol [Fig. 2(b)]. The 60 deg and 30 deg of the space patterns were fabricated on the blocks from A to H. The

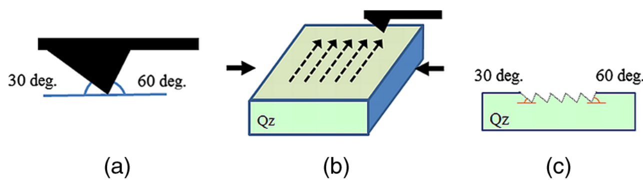

Fig. 1 (a) Schematic view of the cantilever used in the scratching process. The tip angles were 60 deg and 30 deg. (b) Schematic model of the scratching process. The tip made five scratching lines on quartz (Qz) substrate. (c) Cross-sectional profile of the scratched Qz substrate along the line between two arrows indicated in the image (b).

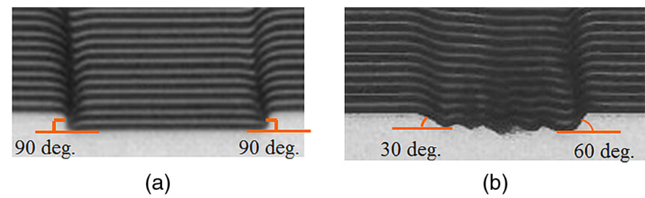

Fig. 3 Cross-sectional TEM images of the space pattern with multilayer (ML). The cross-sectional etching angles were (a) 90 deg. (b) 30 deg and 60 deg.

cross-sectional transmission electron microscope (TEM) images of the fabricated space patterns after their multilayer coating, are shown in Figs. 3(a) and 3(b). Not only the 90 deg of the space pattern but also the 30 deg and 60 deg of the space patterns were robustly fabricated with their etching depths of about 10 nm. The nonflatness of the blank before and after the multilayer coating was <20 nm and −800 nm (center of the multilayer surface was higher than the corners of the blank), respectively.

2.2 *Simulation Condition for the Analysis of the Inclination Angle on the Printed Image*

A simulator known a LAIPH™ EUV Defect Printability Simulator (Luminescent technologies, California) was employed to predict the impact of the inclination angle of the PD on wafer printed image in this work. The parameters for the simulations were as follows: numerical aperture $(\mathrm{NA}) = 0.33$, sigma $= 0.8/0.4$ (dipole), chief ray angle $=$ 6 deg, demagnification $= 4$, and wavelength $= 13.5$ nm. The blank structure was Ru-capped multilayer (Ru $=$ 2.5 nm, 40 pairs of Si/Mo $= 2.8/4.2$ nm). The defect sizes were 4, 6, and 8 nm in depths and 50 nm in full-width at half-maximum. The inclination angles of the PDs were set from −8 deg to 8 deg.

3 Results and Discussion

3.1 *Influence of the Defect Location on the Inclination Angle and its Direction*

To determine the cause of the inclined growth of the PD, space patterns with the etching angles of 90 deg in the blocks A, B, C, D, and G [shown in Fig. 2(a)] were prepared for TEM observation. Figure 4(a) describes a schematic view of the TEM observation direction. Each TEM observation sample was cut perpendicular to the space pattern using a focused ion beam. The TEM images and the inclination angles of the PDs are shown in Fig. 4(b). The inclination angle was defined as the angle between two lines where one line is normal to the substrate surface, and the other is a line defined by connecting the center of the etched substrate to the center of the depressed region (representing a defect image) on the surface of the multilayer. These TEM images clearly show a tendency that the direction of propagation of PDs, starting from the bottom surface of the etched Qz and ending at the top surface of the multilayer, leans toward the center of the mask.

To confirm the tendency of the defect propagation direction, the block H located in the upper-right corner of the mask was prepared for TEM observation. The center-directed space pattern and another space pattern normal to the center-directed space pattern, were both cut perpendicular to the space patterns [Fig. 5(a)]. Figure 5(b) shows the TEM images of the space patterns. The terms TEM-1 and -2 describe the observation directions 1 and 2 depicted in Fig. 5(a). When the space pattern was observed along the direction 1, the inclination angle of the PD was almost 0 deg. However, the space pattern with its direction was normal to the radial direction and was apparently inclined toward the center of the mask (TEM-2). These results indicate that the inclination angle of the PD through the multilayer is not random, but there is a tendency of its propagation direction to lean toward the mask center.

Figure 6 represents a relationship between the inclination angles of the PDs [Figs. 4(b) and 5(b)] and the distances of the space patterns on Qz substrate from the mask center. The inclination angle increased in proportion to the distance from the mask center. The maximum inclination angle was 5.9 deg (93.3 mm away from the mask center).

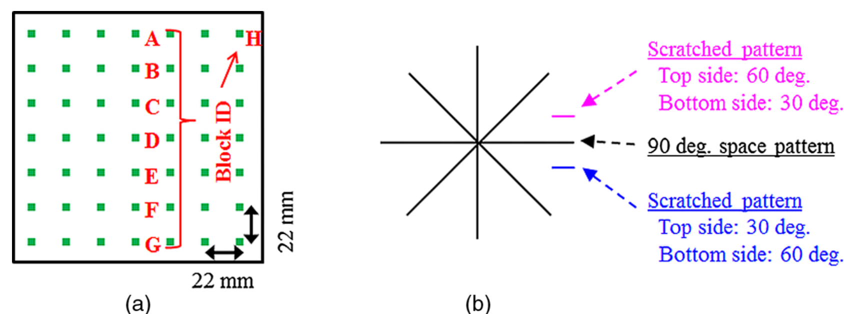

Fig. 2 (a) Arrangement of the test pattern. (b) Magnified image of the each block which has 150 nm of space patterns, forming an asterisk symbol and two types of the scratched patterns.

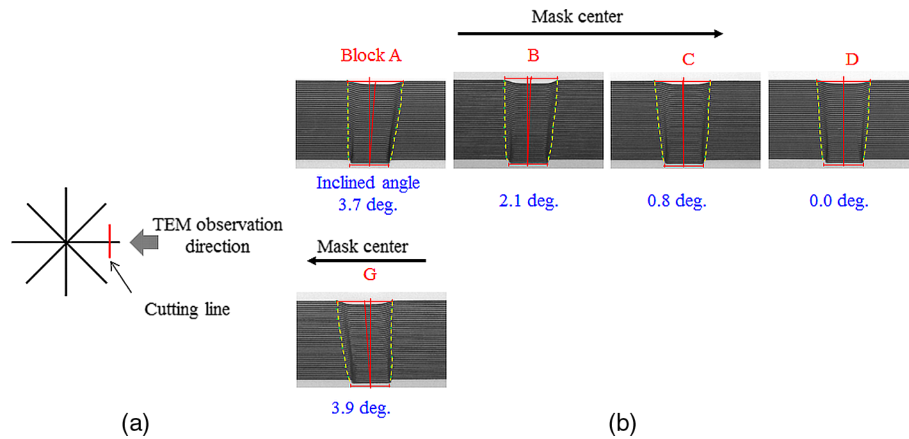

Fig. 4 (a) Explanation of the cutting directions of the space patterns and TEM observation directions. (b) Cross-sectional TEM images of the phase defects (PDs) in the blocks A, B, C, D, and G.

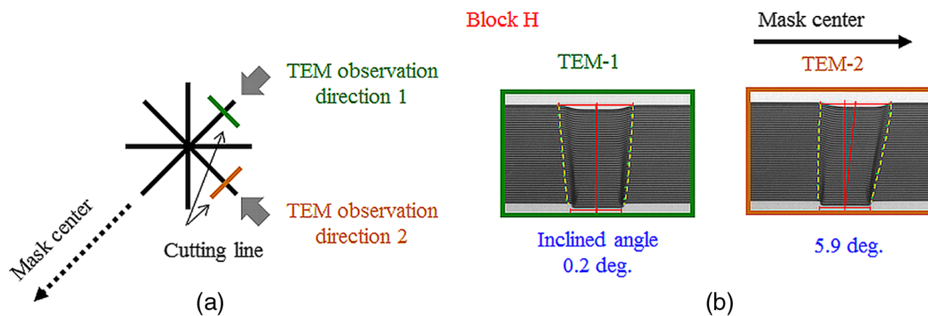

Fig. 5 (a) Explanation of the cutting direction of the space patterns and TEM observation direction. (b) Cross-sectional TEM images of the PDs in the block H.

3.2 *Influence of the Qz Etching Shape on the Propagation Angle of the PD*

To fully understand the defect propagation direction and angle from the bottom to the top of the multilayer, we conducted an investigation to determine the influence of the shapes of the defect seeds on the propagation direction and angle of the PD. Figures 7(a) and 7(b) show the cross-sectional TEM images of the PDs with various shapes of the seeds in the blocks D and A, respectively. The observation results of block D, which were located in the center of the mask, apparently showed that the center of the defect at the bottom and top were completely matched. Furthermore, the observation results of block A, which was located 66 mm from the mask center, also showed that not only the propagation direction but also the inclination angles were independent of the shapes of the seeds on the Qz substrate.

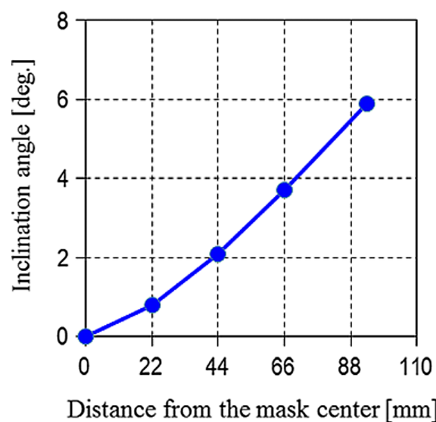

Fig. 6 Inclination angle of the PD through the multilayer as a function of the distance from the mask center.

3.3 *Inclination Angle Versus Positional Shift of the Minimum Intensity of PD Image on Wafer*

The impact of the inclination angel of the PD on the wafer printed image was calculated by a lithography simulator. The simulated mask models were the Ru-capped multilayer with several shapes and sizes of pit-type PDs as described in Sec. 2.2. Figure 8(a) shows the schematic cross-sectional mask structures with vertical-type and inclined-type pit PDs. The defects were 6-nm deep and 50-nm wide with their inclination angles of 0 deg and 8 deg. The calculated wafer printed images are shown in Fig. 8(b). Compared with the wafer printed image of the vertical-type PD, the inclined-type PD image shifted about 8 nm on the mask scale, which corresponded to 2 nm on the wafer scale.

The calculated positional shift of the PD image on the wafer due to the inclination angles are summarized in

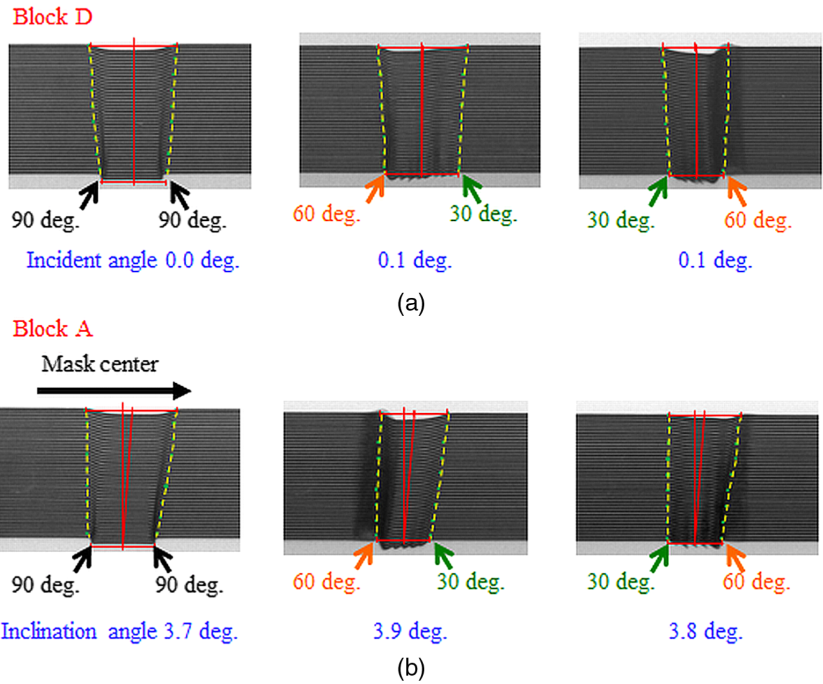

Fig. 7 Cross-sectional TEM images of the (a) block D and (b) block A. The etching angles of the Qz substrate are 30 deg, 60 deg, and 90 deg.

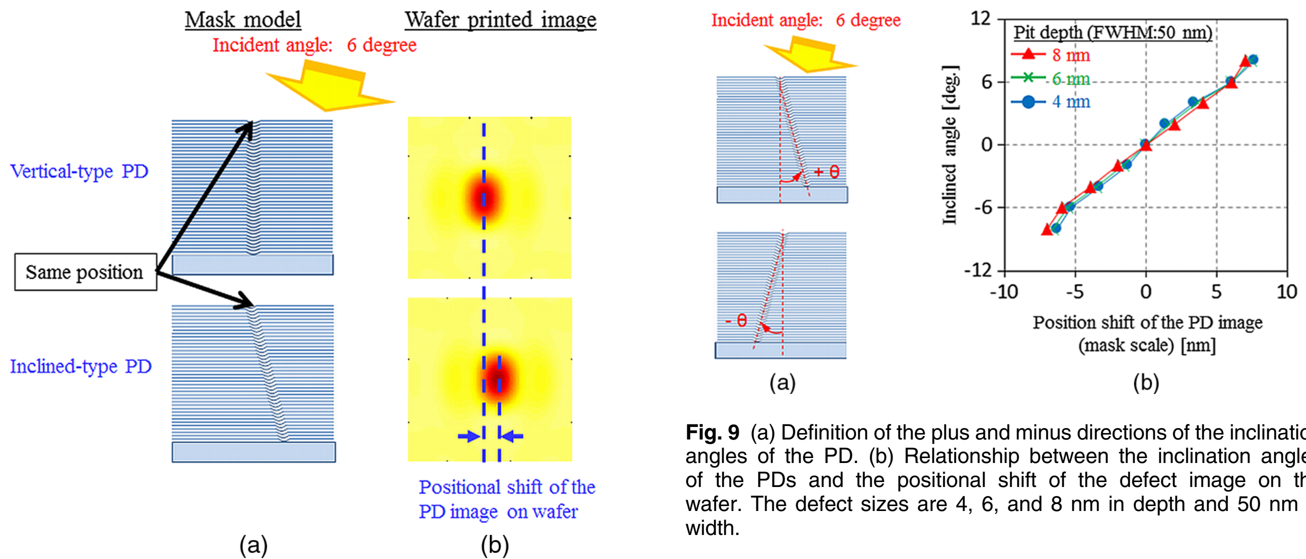

Fig. 8 (a) Cross-sectional schematic view of the masks with vertical-type PD and inclined-type PD. (b) Calculated wafer printed images of the PDs.

Fig. 9 (a) Definition of the plus and minus directions of the inclination angles of the PD. (b) Relationship between the inclination angles of the PDs and the positional shift of the defect image on the wafer. The defect sizes are 4, 6, and 8 nm in depth and 50 nm in width.

Fig. 9. The plus or minus of the inclination angles are defined as shown in Fig. 9(a) with a definition of EUV incident direction and angle. Figure 9(b) shows the positional shifts of the PD images on the wafer as a function of the inclination angle of the PDs. The results show that the image shift values are independent of the depths of the pit-type defects. The image of the inclined PD on wafer shifts about 1 nm/deg to the inclined direction compared with the vertical-types one.

4 Summary and Conclusion

Various shapes of the space patterns were fabricated on the surface of a Qz substrate using an AFM scratching process and a mask patterning process. The Qz substrate was coated with a multilayer for defect propagation analysis from the surface of the Qz substrate to the surface of the multilayer. Propagations of the surface topography of the Qz through the multilayer were observed by a TEM. An incident angle of 5.9 deg was observed at a distance of 93 mm away from the mask center. The inclination angle of the defect was independent of the shape of the defect seed on the Qz substrate. A PD with an inclination angle of 1 deg corresponded to a positional shift of image of 1 nm on a printed wafer image.

Acknowledgments

The authors would like to acknowledge Osamu Takaoka and Fumio Aramaki of Hitachi High-Tech Science Corporation for their technical support of scratching of the Qz substrate using their AFM type mask repair tool SPR6300. This work was supported by New Energy and Industrial Technology Development Organization (NEDO).

References

1. T. Terasawa et al., "Phase defect printability and actinic dark-field mask blank inspection capability analyses," *Proc. SPIE* **7969**, 79690V (2011).
2. T. Terasawa et al., "Actinic phase defect detection and printability analysis for patterned EUVL mask," *Proc. SPIE* **7636**, 763602 (2010).
3. D. V. Heuvel et al., "Natural EUV mask blank defects: evidence, timely detection, analysis and outlook," *Proc. SPIE* **7823**, 78231T (2010).
4. R. Jonckheere et al., "Evidence of printing blank-related defects on EUV masks missed by blank inspection," *Proc. SPIE* **7985**, 79850W (2011).
5. R. Jonckheere et al., "Additional evidence of EUV blank defects first seen by wafer printing," *Proc. SPIE* **8166**, 81660E (2011).
6. A. Erdmann et al., "Analysis of EUV mask multilayer defect printing characteristics," *Proc. SPIE* **8322**, 83220E (2011).
7. G. Zhang et al., "EUV mask readiness for high volume manufacturing," in *2010 Int. Symp. Extreme Ultraviolet Lithography*, Sematech, Kobe, Japan (2010).
8. Y. Du et al., "Linear time EUV blank defect mitigation algorithm considering tolerance to inspection inaccuracy," *Proc. SPIE* **8522**, 85221R (2012).
9. T. Onoue et al., "Development of fiducial marks on EUV blanks for defect mitigation process," *Proc. SPIE* **8322**, 832226 (2012).
10. T. Murachi et al., "Registration accuracy improvement of fiducial mark on EUVL mask with MIRAI EUV ABI prototype," *Proc. SPIE* **8679**, 86791U (2013).
11. T. Murachi et al., "Fiducial mark requirements from the viewpoints of actinic blank inspection tool for phase-defect mitigation on EUVL mask," *Proc. SPIE* **8522**, 85221U (2012).
12. T. Murachi et al., "Phase defect mitigation strategy: fiducial mark requirements on extreme ultraviolet lithography mask," *Proc. SPIE* **8322**, 83221Q (2012).
13. R. Jonckheere et al., "Progress forwards defect-free EUV reticles for NXE:3100," in *2011 Int. Symp. Extreme Ultraviolet Lithography*, Sematech, Miami, Florida (2011).
14. R. F. Spivey et al., "Development of 3D Monte Carlo simulations for predicting multilayer geometry of pit-type EUV defects," *Proc. SPIE* **8679**, 86791W (2013).
15. H. J. Kwon et al., "Printability of native blank defects and programmed defects and their stack structures," *Proc. SPIE* **8166**, 81660H (2011).
16. T. Amano et al., "Impact of the phase defect structure on an actinic dark-field blank inspection signal and wafer printability," *Proc. SPIE* **8322**, 832234 (2012).
17. A. Rastegar et al., "EUV mask defects and their removal," *Proc. SPIE* **8352**, 83520W (2012).
18. V. Jindal et al., "Modeling the EUV multilayer deposition process on EUV blanks," *Proc. SPIE* **7969**, 79691A (2011).
19. H. Miyai et al., "EUV actinic blank inspection tool development," in *2011 Int. Symp. Extreme Ultraviolet Lithography*, Sematech, Miami, Florida (2011).

Tsuyoshi Amano received his BS and MS degrees in applied chemistry from Keio University in 1997 and 1999, respectively. He joined Dai Nippon Printing Co. Ltd., where he carried out research on mask process, metrology, and repair technology. In 2011, he was assigned to EUVL Infrastructure Development Center, Inc. (EIDEC) and since then he has been engaged in the development of patterned masks and blank inspection tools.

Biography and photograph of the other author are not available.